ChemPubSoc Europe
DOI: 10.1002/cctc.201402970
CHEMCATCHEM
Full Papers

Role of Vanadium and Phosphorus in Substituted Keggin-Type Heteropolyoxo Molybdates Supported on Silica SBA-15 in Selective Propene Oxidation

Rafael Zubrzycki, Jan Dirk Epping, and Thorsten Ressler*[a]

Vanadium-containing Keggin-type heteropolyoxo molybdate ($[PV_2Mo_{10}O_{40}]^{5-}$) was supported on silica SBA-15 (denoted as PV_2Mo_{10}-SBA-15). The structural evolution and catalytic activity of PV_2Mo_{10}-SBA-15 and a suitable reference $V_2Mo_{10}O_x$-SBA-15 were investigated under selective propene oxidation conditions by using in situ X-ray absorption spectroscopy. ^{31}P MAS NMR measurements of supported PV_2Mo_{10}-SBA-15 and reference H_3PO_4-SBA-15 were performed after the catalytic reaction. PV_2Mo_{10}-SBA-15 formed a mixture of mainly tetrahedral $[MoO_x]$ and $[VO_x]$ units during thermal treatment under propene oxidation conditions. Changes in the average local structure around V centers coincided with the changes in the average local structure around Mo centers and the onset of catalytic activity. In addition, mainly tetrahedral $[MoO_x]$ and $[VO_x]$ units seemed to be in close proximity and interacted under catalytic conditions. Conversely, in the reference material $V_2Mo_{10}O_x$-SBA-15 synthesized with individual V and Mo source precursors, Mo and V centers appeared to be more separated from each other. The structural environment of P in PV_2Mo_{10}-SBA-15 under catalytic conditions corresponded to a mixture of various species. P was connected to both the support material SBA-15 via P—O—Si bonds and $[MoO_x]$ or $[VO_x]$ units. Apparently, the proximity of V and Mo in Keggin precursors was a prerequisite for obtaining (Mo,V) oxide species on the support material.

Introduction

Molybdenum oxides constitute active heterogeneous catalysts for the selective oxidation of alkenes and alkanes with gas phase oxygen.[1–3] However, α-MoO_3 exhibits only poor catalytic activity and selectivity. Varying the chemical composition results in more active mixed metal oxide catalysts for the oxidation of propene to acrolein or acrylic acid. The addition of V, W, Nb, or Te yields mixed oxides with various characteristic structures and catalytic functionalities. However, elucidating structure–activity relationships is often hindered by simultaneously varying composition and structure. Moreover, the functionality of individual metal centers or particular structural motifs of these highly active mixed oxide catalysts can hardly be determined. Hence, model systems that combine structural invariance with compositional variety are required. Heteropolyoxo molybdates (HPOMs) with a Keggin structure exhibit a broad compositional range while maintaining their characteristic structural motifs.[4–6] Substituting Mo atoms with addenda atoms (i.e., V, W, or Nb) make Keggin-type HPOM a suitable model system to study structure–activity relationships. Moreover, P- and V-containing catalysts are active and selective in oxidative dehydrogenation (ODH) reactions, which possibly exhibit similar functionalities as catalysts for selective propene oxidation.[7,8] Thus, HPOMs have been frequently studied as active catalysts for selective oxidation reactions.[9] Incorporating V atoms in bulk HPOM leads to a decreasing thermal stability.[10] Keggin ions partially decompose under catalytic conditions above 573 K to form lacunary Keggin anions in which Mo cations migrate to extra Keggin ion sites. Driving force for the formation of lacunary Keggin anions may be the relaxation of the Keggin structure at an elevated temperature upon removal of structural water. Subsequently, links are formed between Keggin ions, which eventually resulted in more extended oxide structures.[6,11]

In addition to using bulk model catalysts for determining structure–activity relationships, supported metal oxide catalysts have received increasing attention.[12,13] The supported catalytic species have higher dispersion and an improved surface to bulk ratio. Hence, differentiating between bulk and surface structures is no longer necessary. Therefore, structure–activity relationships can be readily deduced from the characteristic oxide species observed on the support material under catalytic reaction conditions. Suitable support materials for catalyst model systems should have a large surface area and a homogeneous internal structure with sufficiently large pores. Furthermore, the support should interact with the precursor to stabilize particular structural motifs without being involved in the catalytic reaction. Nanostructured SiO_2 materials such as SBA-15[14,15] represent suitable support systems for oxide catalysts.[16,17] Supported HPOMs combine the possibility of varying the chemical compositions with the good accessibility of supported Mo-based catalysts.

Keggin-type $H_4[PVMo_{11}O_{40}]$ has been reported to exhibit a pronounced interaction effect with SBA-15 as the support

---

[a] R. Zubrzycki, Dr. J. D. Epping, Prof. T. Ressler
Department of Chemistry
Technische Universität Berlin
Strasse des 17. Juni 135, 10623 Berlin (Germany)
E-mail: thorsten.ressler@tu-berlin.de

material.[18] This effect resulted in a further decreased thermal stability of the supported Keggin ions compared with the bulk materials. Under catalytic conditions, $PVMo_{11}$-SBA-15 formed a mixture of tetrahedrally and octahedrally coordinated $[MoO_4]$ and $[MoO_6]$ units.[18] However, the role and structural evolution of V and P in the supported HPOMs under catalytic conditions remained largely unknown.

Herein, we present in situ X-ray absorption spectroscopy investigations performed at the V K edge of PV_2Mo_{10}-SBA-15 under propene oxidation conditions. Moreover, ^{31}P MAS NMR measurements of supported PV_2Mo_{10}-SBA-15 and reference H_3PO_4 supported on SBA-15 (denoted as H_3PO_4-SBA-15) after the catalytic oxidation of propene are described. Correlations between the structural evolution of $[MoO_x]$ and $[VO_x]$ units and performance under catalytic conditions are also presented.

Results and Discussion

Long-range structure of the as-prepared PV_2Mo_{10}-SBA-15

The long-range structure of the as-prepared PV_2Mo_{10}-SBA-15 was investigated by using small-angle and wide-angle XRD (Figure 1). At small angles, SBA-15 and PV_2Mo_{10}-SBA-15 exhibited the characteristic patterns representing the hexagonal pore structure of nanostructured SBA-15. A lattice constant of the hexagonal unit cell of $a = 12.1$ nm of both SBA-15 and PV_2Mo_{10}-SBA-15 was determined from the (10 *l*) peak. SBA-15 had a BET surface area of 877 m^2g^{-1}. BJH calculations of pore size distributions resulted in a pore diameter of $d_{pore} = 10.6$ nm. Given the pore diameter and lattice constant, the wall thickness of the SBA-15 material used amounted to approximately 2 nm. In contrast to the wide-angle XRD patterns of a mechanical mixture of bulk $H_5[PV_2Mo_{10}O_{40}]\cdot 13H_2O$ and SBA-15 with a ratio of 10 wt%, the pattern of $PV_2Mo_{10}O_{40}$-SBA-15 showed no long-range ordered molybdenum oxide species. This indicated sufficiently dispersed Keggin ions without the formation of extended crystalline HPOM structures.

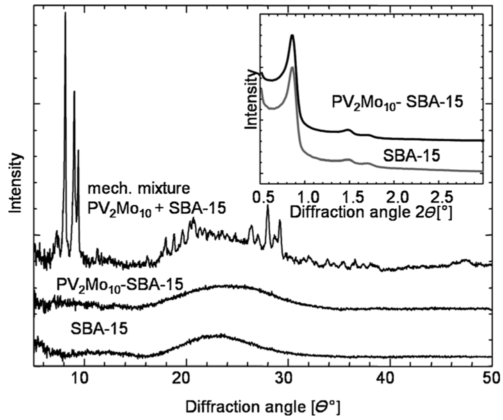

Figure 1. Wide-angle and small-angle (inset) XRD patterns of PV_2Mo_{10}-SBA-15, SBA-15, and a mechanical mixture of PV_2Mo_{10} and SBA-15.

Short-range-order structural characterization of PV_2Mo_{10}-SBA-15

The V K-edge FT($\chi(k)\cdot k^3$) of PV_2Mo_{10}-SBA-15 and bulk PV_2Mo_{10} is shown in Figure 2a. The typical Mo K-edge FT($\chi(k)\cdot k^3$) of PV_2Mo_{10}-SBA-15, $PVMo_{11}$-SBA-15, PV_2Mo_{10}, and $PVMo_{11}$ is shown in Figure 2b.[6,19] The similar shape of the FT($\chi(k)\cdot k^3$) indicated a similar local structure around V and Mo centers in the unsupported and supported HPOM Keggin structure. Supporting PV_2Mo_{10} on SBA-15 resulted in a decreased amplitude of the corresponding V K-edge FT($\chi(k)\cdot k^3$). Conversely, the Mo K-edge FT($\chi(k)\cdot k^3$) of PV_2Mo_{10}-SBA-15 and $PVMo_{11}$-SBA-15 showed an increasing amplitude. This increase in amplitude of the FT($\chi(k)\cdot k^3$) in the range between 2.5 and 3.8 Å was previously reported for $PVMo_{11}$ and $PVMo_{11}$-SBA-15.[18] Eventually, the Mo and V K-edge FT($\chi(k)\cdot k^3$) confirmed that the Keggin ion structure motif was maintained upon supporting PV_2Mo_{10} on SBA-15. The V and Mo K-edge X-ray absorption near-edge structure (XANES) spectra of the as-prepared PV_2Mo_{10}-SBA-15 and activated PV_2Mo_{10}-SBA-15 after thermal treatment in 5% propene and 5% oxygen in He at 723 K are shown in Figure 3. The V and Mo K-edge XANES spectra of PV_2Mo_{10} and PV_2Mo_{10}-SBA-15 showed similar features. An analysis of the Mo K-edge position[20] yielded an average valence of approximately 6. Comparing the pre-edge peak at the V K edge of PV_2Mo_{10}-SBA-15 and

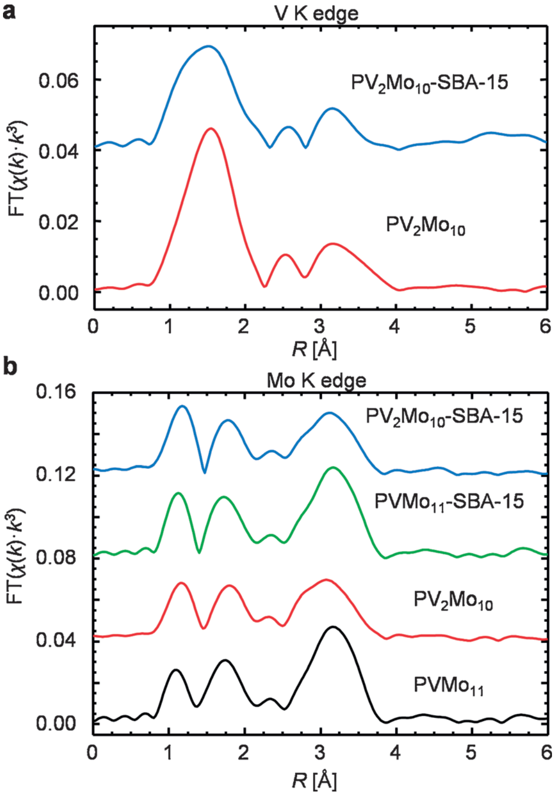

Figure 2. a) V K-edge FT($\chi(k)\cdot k^3$) of $H_5[PV_2Mo_{10}O_{40}]$ (PV_2Mo_{10}) and $H_5[PV_2Mo_{10}O_{40}]$ supported on SBA-15 (PV_2Mo_{10}-SBA-15) and b) Mo K-edge FT($\chi(k)\cdot k^3$) of $PVMo_{11}$ ($H_4[PVMo_{11}O_{40}]$) and PV_2Mo_{10} ($H_5[PV_2Mo_{10}O_{40}]$) and HPOMs supported on SBA-15 ($PVMo_{11}$-SBA-15 and PV_2Mo_{10}-SBA-15).

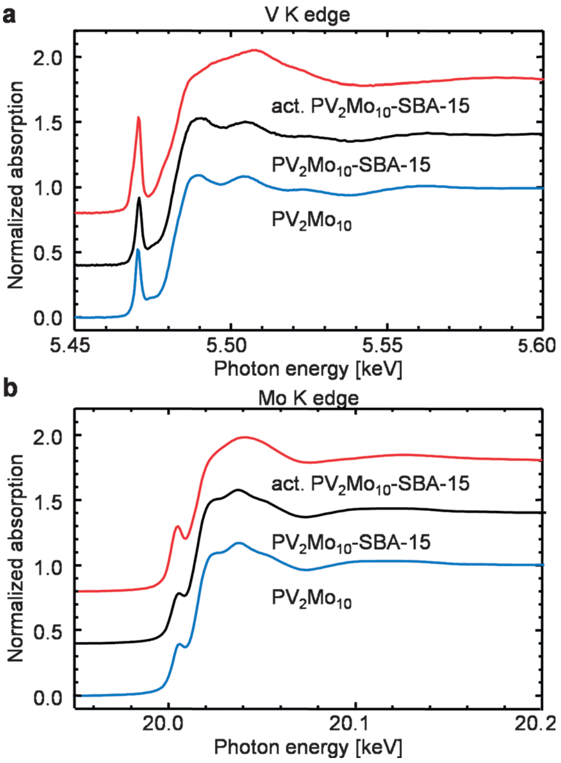

Figure 3. a) V K-edge XANES of PV_2Mo_{10}, PV_2Mo_{10}-SBA-15, and activated PV_2Mo_{10}-SBA-15 and b) Mo K-edge XANES of PV_2Mo_{10}, PV_2Mo_{10}-SBA-15, and activated PV_2Mo_{10}-SBA-15 after thermal treatment in 5 % propene and 5 % oxygen at 723 K.

vanadium oxide as the reference compound indicated an average V valence between 4 and 5.

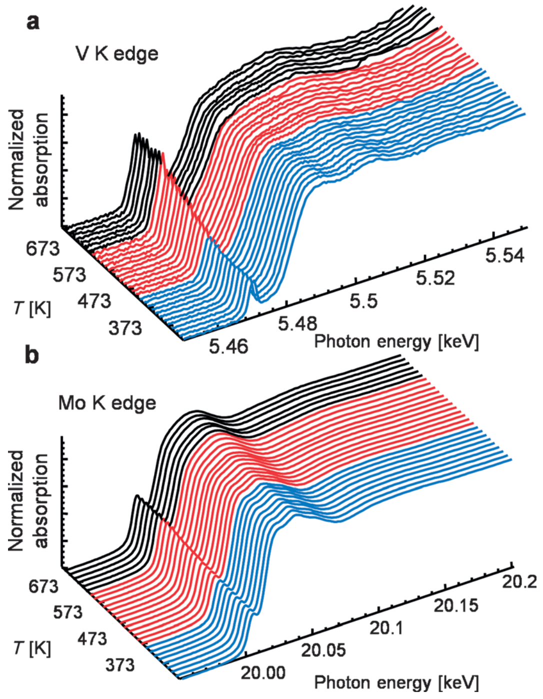

Figure 4. a) In situ V K-edge XANES spectra and b) in situ Mo K-edge XANES spectra of PV_2Mo_{10}-SBA-15 during temperature-programmed treatment in 5 % propene and 5 % oxygen in He in the temperature range 300–723 K.

Structural evolution of PV_2Mo_{12}-SBA-15 under catalytic conditions

PV_2Mo_{10}-SBA-15 was investigated by using in situ XAS under catalytic conditions. The evolution of V and Mo XANES spectra of PV_2Mo_{10}-SBA-15 during temperature-programmed treatment in 5 % propene and 5 % oxygen are shown in Figure 4 a and b, respectively. The pre-edge peak features can be used to elucidate the average local structure around metal centers. Using the pre-edge peak height sufficed to quantify the contribution of tetrahedral [MO_4] and distorted [MO_6] (M = V, Mo) units present during the thermal treatment of the catalysts. The pre-edge peak heights of in situ V and Mo K-edge XANES spectra at 298 K (Figure 4) were attributed to the distorted MO_6 (M = V, Mo) building units of the Keggin ion with the metal centers in their highest oxidation states.[5,21] The XANES spectra remained unchanged in the temperature range 298–473 K. Hence, the Keggin structure appeared to be stable up to 473 K. Between 473 and 648 K, the pre-edge peak height increased with temperature. This indicated structural changes from octahedral to tetrahedral [MO_x] (M = V, Mo) units during thermal treatment under catalytic conditions.[22,23] The evolution of the normalized pre-edge peak height together with the ion currents of H_2O, CO, CO_2, acrolein, and acetone during the oxidation of propene is shown in Figure 5 b. The in situ Mo K-edge FT($\chi(k)\cdot k^3$) (Figure 5 a) indicated that the Keggin structure was intact up to 473 K. Structural changes observed in the Mo K-edge FT($\chi(k)\cdot k^3$) between 473 and 648 K coincided with the evolution of the pre-edge peak height of V and Mo K edge of PV_2Mo_{10}-SBA-15. No structural changes in the FT($\chi(k)\cdot k^3$) of Mo could be determined above 648 K. Moreover, changes in pre-edge heights of V and Mo occurred on the same time scale, which thus confirmed the incorporation of V centers in the Keggin structure. The onset of catalytic activity and the formation of various selective oxidation products coincided with the detected structural changes. Apparently, the catalytically active species formed during thermal activation from the original Keggin structure under reaction conditions. These active species mainly consist of V and Mo centers in partial tetrahedral coordination.

Average local structure around Mo centers in activated PV_2Mo_{10}-SBA-15 and reference $V_2Mo_{10}O_x$-SBA-15 under catalytic conditions

The Mo K-edge FT($\chi(k)\cdot k^3$) of activated PV_2Mo_{10}-SBA-15 and activated $V_2Mo_{10}O_x$-SBA-15 after thermal treatment under catalytic conditions is shown in Figure 6. The FT($\chi(k)\cdot k^3$) of activated PV_2Mo_{10}-SBA-15 exhibited features similar to that of previously reported dehydrated molybdenum oxides and HPOMs supported on SBA-15.[18,23] For a more detailed analysis, hexagonal MoO_3 was used as a structural model. Theoretical X-ray absorption fine structure (XAFS) phases and amplitudes were calculated for Mo–O and Mo–Mo distances and used for extended X-

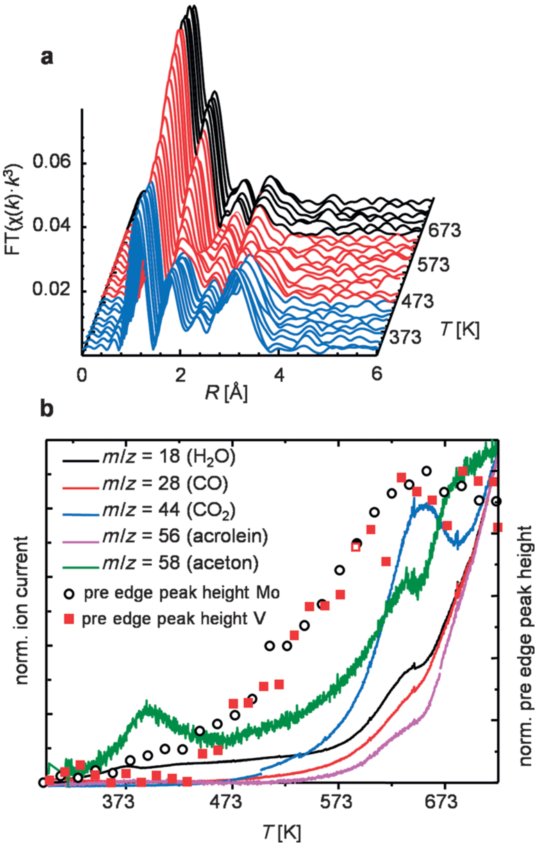

Figure 5. a) In situ evolution of Mo K-edge FT($\chi(k)\cdot k^3$) of PV_2Mo_{10}-SBA-15 during thermal treatment in 5 % propene and 5 % oxygen in He in the temperature range 303–723 K (heating rate: 4 K min^{-1}) and b) evolution of the normalized ion current of H_2O (m/z 18), CO (m/z 28), CO_2 (m/z 44), acrolein (m/z 56), and acetone (m/z 58) and normalized pre-edge height of V and Mo K edge of PV_2Mo_{10}-SBA-15 during thermal treatment in 5 % propene and 5 % oxygen in He in the temperature range 303–723 K (heating rate: 4 K min^{-1}).

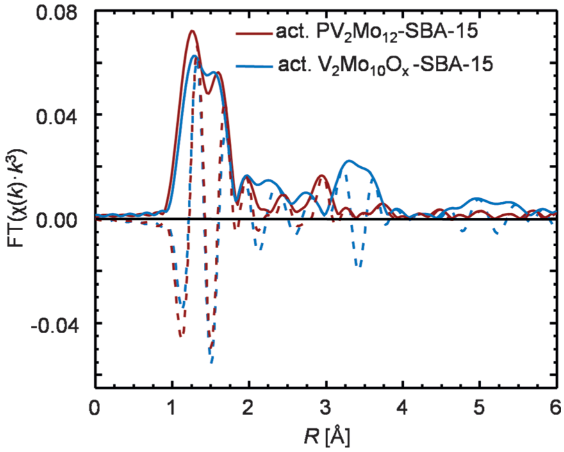

Figure 6. Mo K-edge FT($\chi(k)\cdot k^3$) of activated PV_2Mo_{10}-SBA-15 and activated $V_2Mo_{10}O_x$-SBA-15 after thermal treatment in 5 % propene and 5 % oxygen in He at 723 K.

Table 1. Type, number (*N*), and XAFS disorder parameters (σ^2) of atoms at a distance *R* from the Mo atoms in activated PV_2Mo_{10}-SBA-15 and activated $V_2Mo_{10}O_x$-SBA-15.[a]

Type	Activated PV_2Mo_{11}-SBA-15 *N*	*R* [Å]	σ^2 [Å^2]	Type	Activated $V_2Mo_{10}O_x$-SBA-15 *N*	*R* [Å]	σ^2 [Å^2]
Mo–O	2	1.67	0.0013	Mo–O	2	1.68	0.0023
Mo–O	2	1.88	0.0034	Mo–O	2	1.90	0.0042
Mo–O	1	2.18	0.0034_c	Mo–O	1	2.11	0.0042_c
Mo–O	1	2.34	0.0017	Mo–O	1	2.34	0.0001
Mo–Mo	–	–	–	Mo–Mo	–	3.14	0.0061
Mo–Mo	2	3.49	0.0061	Mo–Mo	2	3.28	0.0061_c
Mo–Mo	2	3.63	0.0061_c	Mo–Mo	2	3.71	0.0057
Mo–Mo	2	3.75	0.0100	Mo–Mo	2	3.92	0.0113

[a] Experimental parameters were obtained from a refinement of a hexagonal MoO_3 model structure (ICSD no. 75417) to the experimental Mo K-edge XAFS $\chi(k)$ function of activated PV_2Mo_{10}-SBA-15 (*k* range: 3.6–16.0 Å^{-1}, *R* range: 0.9–4.0 Å, $E_0 \approx$-5.2, residual ≈ 12.8, $N_{ind} = 27$, $N_{free} = 12$) and activated $V_2Mo_{10}O_x$-SBA-15 (*k* range: 3.6–16.0 Å^{-1}, *R* range: 0.9–4 Å, $E_0 \approx -0.4$, residual ≈ 10.9, $N_{ind} = 26$, $N_{free} = 14$). Subscript c indicates parameters that were correlated in the refinement.

ray absorption fine structure (EXAFS) refinement. The results of the refinement are summarized in Table 1. Distinct changes in the first Mo–O coordination sphere indicated a change in Mo–O distance distribution or coordination geometry. Higher Mo–Mo peaks in the FT($\chi(k)\cdot k^3$) exhibited a decreased amplitude caused by an increased dispersion of Mo species on silica SBA-15 after thermal treatment under catalytic conditions. A distinct peak at approximately 3 Å in the FT($\chi(k)\cdot k^3$) indicated the formation of dimeric or oligomeric [Mo_xO_y] units on SBA-15.

Hence, isolated tetrahedral [MoO_4] units can be excluded as major molybdenum oxide species.[24] Linear combinations of the XANES spectra of Na_2MoO_4 and MoO_3 references were used to determine the amount of tetrahedral [MoO_4] and octahedral [MoO_6] units in activated PV_2Mo_{10}-SBA-15 and activated $V_2Mo_{10}O_x$-SBA-15. Apparently, activated PV_2Mo_{10}-SBA-15 consisted of a mixture of tetrahedral [MoO_4] and octahedral [MoO_6] units in a ratio of 2:1. For activated $V_2Mo_{10}O_x$-SBA-15, a ratio of 1:1 was found. A comparison of the pseudo radial distribution functions of activated $V_2Mo_{10}O_x$-SBA-15 and activated PV_2Mo_{10}-SBA-15 confirmed the results of the XANES analysis. The first peak of the Mo K-edge FT($\chi(k)\cdot k^3$) of activated $V_2Mo_{10}O_x$-SBA-15 differed from that of activated PV_2Mo_{10}-SBA-15. The first peak in both FT($\chi(k)\cdot k^3$) originated mainly from the tetrahedral species on the SBA-15 support and could be sufficiently simulated using four Mo–O distances. These four distances sufficiently accounted for the minor amount of octahedral [MoO_6] species. The first and second disorder parameters (1st-σ^2 and 2nd-σ^2) were higher for activated $V_2Mo_{10}O_x$-SBA-15 and indicated a decreased amount of tetrahedral [MoO_4] units. The third Mo–O distance was considerably shorter than the distance in activated PV_2Mo_{10}-SBA-15. In addition, the fourth disorder parameter (4th-σ^2) for $V_2Mo_{10}O_x$-SBA-15 was smaller than the fourth disorder parameter (4th-σ^2) for activated PV_2Mo_{10}-SBA-15. This disorder parameter mainly represented the fraction of octahedral [MoO_6] units. Hence, the reduced disorder parameter indicated an increasing amount of octahedral structural motifs in activated $V_2Mo_{10}O_x$-SBA-15 compared to activated PV_2Mo_{10}-SBA-15. Furthermore, the amplitude in the Mo K-edge $FT(\chi(k)\cdot k^3)$ of activated $V_2Mo_{10}O_x$-SBA-15 at higher Mo–Mo peaks resembled the shape of α-MoO_3. The Mo–Mo distance at approximately 3.3 Å is characteristic of α-MoO_3. These results confirmed the existence of crystalline α-MoO_3, which was also identified by XRD before thermal treatment under catalytic conditions. Estimating the amount of α-MoO_3 from the amplitude at approximately 3.3 Å in the pseudo radial distribution function yielded an amount of approximately 20 %.

Average local structure around V centers in activated PV_2Mo_{10}-SBA-15 and reference $V_2Mo_{10}O_x$-SBA-15 under catalytic conditions

The evolution of the average local structure around V centers in the supported catalysts and reference materials differed from that around Mo centers. The V K-edge $FT(\chi(k)\cdot k^3)$ of activated $V_2Mo_{10}O_x$-SBA-15 and activated PV_2Mo_{10}-SBA-15 is shown in Figure 7. The amplitudes at distances between 3 and 4 Å indicated different backscattering atoms. Single scattering paths of a $Na_2Mo_2O_7$ structure (ICSD no. 24312[25]) were used for the EXAFS refinement of activated $V_2Mo_{10}O_x$-SBA-15 and activated PV_2Mo_{10}-SBA-15. The theoretical model structure of activated PV_2Mo_{10}-SBA-15 was based on the $Na_2Mo_2O_7$ structure with one Mo atom replaced by one V atom per formula unit. The results of the refinements for the V K-edge $FT(\chi(k)\cdot k^3)$ are given in Table 2. The distances between 1 and 2 Å corresponded to a tetrahedral $[VO_4]$ unit. Distances R and disorder parameters σ^2 were nearly identical for activated PV_2Mo_{10}-SBA-15 and activated $V_2Mo_{10}O_x$-SBA-15 (Figures 8 and 9). The first Mo coordination sphere corresponded to a mixture of octahedral and mainly tetrahedral $[MoO_x]$ species. In contrast to the first Mo–O peak with six individual Mo–O distances, the first V–O peak could be sufficiently simulated with four individual V–O distances. Si atoms from the support were found at a distance of approximately 2.55 Å. In addition, a V–Mo distance was identified in the V K-edge $FT(\chi(k)\cdot k^3)$ of activated PV_2Mo_{10}-SBA-15. V–O and V–V distances in activated $V_2Mo_{10}O_x$-SBA-15 were similar to those in dehydrated V_xO_y-SBA-15 synthesized with a butylammonium decavanadate precursor.[22] Assume that only V–V distances resulted in a sufficient agreement between experimental and theoretical spectra in contrast to activated PV_2Mo_{10}-SBA-15. This indicated that $[VO_x]$ and $[MoO_x]$ species were not present in close proximity to each other. The results of Mo and V K-edge analyses of activated PV_2Mo_{10}-SBA-15 and activated $V_2Mo_{10}O_x$-SBA-15 confirmed that only activated PV_2Mo_{10}-SBA-15 contained supported V–O–Mo mixed oxide structural motifs formed under catalytic conditions.

Table 2. Type, number (N), and XAFS disorder parameters (σ^2) of atoms at a distance R from the V atoms in activated PV_2Mo_{10}-SBA-15 and activated $V_2Mo_{10}O_x$-SBA-15.[a]

Type	Activated PV_2Mo_{10}-SBA-15 N	R [Å]	σ^2 [Å^2]	Type	Activated $V_2Mo_{10}O_x$-SBA-15 N	R [Å]	σ^2 [Å^2]
V–O	2	1.83	0.0183	V–O	2	1.82	0.0160
V–O	2	1.83_c	0.0183_c	V–O	2	1.82_c	0.0160_c
V–Si	1	2.54	0.0172	V–Si	1	2.55	0.0094
V–O	1	2.91	0.005_f	V–O	1	2.95	0.0046_f
V–O	1	3.10	0.0246	V–V	1	3.30	0.0089
V–Mo	1	3.60	0.0221	V–V	1	3.58	0.0089_c

[a] Experimental parameters were obtained from a refinement of a modified $[Mo_2O_7]^{2-}$ model system (ICSD no. 24312), in which Mo was replaced by V and Si was additional added compared to the experimental V K-edge XAFS $\chi(k)$ of activated $V_2Mo_{10}O_x$-SBA-15 (Figure 8; k range: 3.0–10.0 Å^{-1}, R range: 0.9–3.8 Å, $E_0 \approx 8.8$, residual ≈ 11.3, $N_{ind} = 13$, $N_{free} = 8$) and activated PV_2Mo_{10}-SBA-15 (Figure 9; k range: 3.0–10.0 Å^{-1}, R range: 0.9–3.8 Å, $E_0 \approx 8.8$, residual ≈ 6.0, $N_{ind} = 13$, $N_{free} = 8$). Subscript c indicates parameters that were correlated and subscript f indicates parameters that were fixed in the refinement.

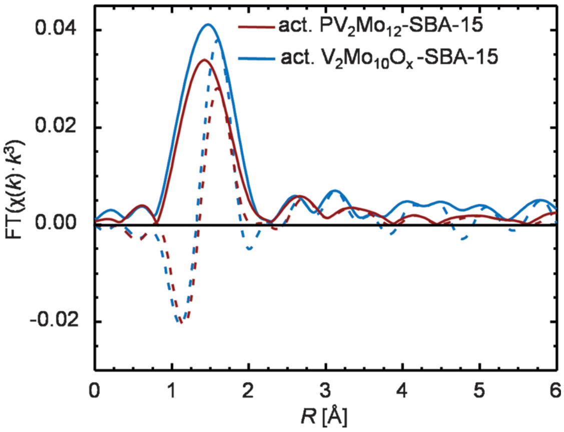

Figure 7. V K-edge $FT(\chi(k)\cdot k^3)$ of activated PV_2Mo_{10}-SBA-15 and activated $V_2Mo_{10}O_x$-SBA-15 after thermal treatment in 5 % propene and 5 % oxygen in He at 723 K.

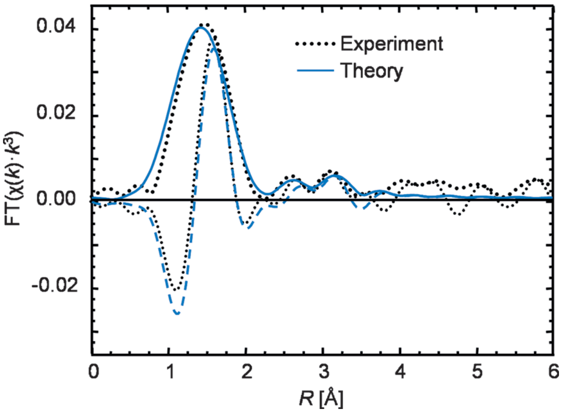

Figure 8. Theoretical and experimental V K-edge $FT(\chi(k)\cdot k^3)$ of activated $V_2Mo_{10}O_x$-SBA-15. Structural parameters are given in Table 2.

Active sites of selective oxidation catalysts often consist of multiple metal atoms.[26] Synthesis routes of supported ternary oxides with different metal oxide precursors have rarely been reported. V-substituted Keggin ions enabled the synthesis of connected $[VO_x]$ and $[MoO_x]$ species not readily available from

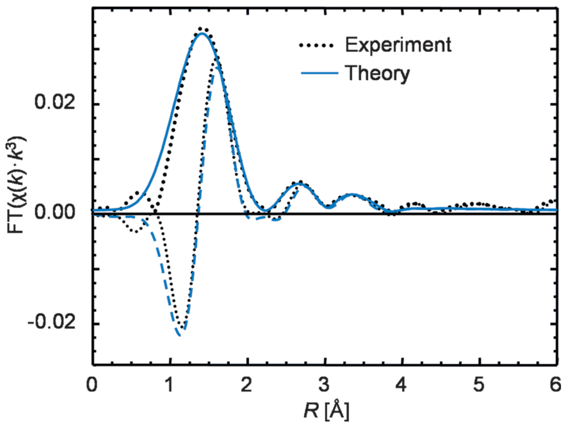

Figure 9. Theoretical and experimental V K-edge FT($\chi(k)\cdot k^3$) of activated PV_2Mo_{10}-SBA-15. Structural parameters are given in Table 2.

physically mixed precursors. Apparently, the proximity of V and Mo in Keggin precursors is a prerequisite for obtaining connected metal oxide species on the support material SBA-15.

Local structure of P in activated PV_2Mo_{10}SBA-15 under catalytic conditions

The ^{31}P MAS NMR spectra of the as-prepared and activated PV_2Mo_{10}-SBA-15 in comparison to the as-prepared and activated reference H_3PO_4-SBA-15 are shown in Figure 10. The ^{31}P MAS NMR spectrum of PV_2Mo_{10}-SBA-15 resembled that of bulk $PVMo_{11}$.[27] This confirmed that the majority of P centers was located in Keggin ions supported on SBA-15.[28] The peak in the spectrum of H_3PO_4-SBA-15 at 0.8 ppm could be assigned to molecular H_3PO_4. In the spectrum of activated H_3PO_4-SBA-15, four pronounced peaks can be seen at chemical shifts of 0.8, −10.8, −22.8, and −35.9 ppm. Zhang and coworkers reported similar results for SiO_2 impregnated with H_3PO_4.[29,30] Accordingly, the peak at 0.1 ppm is characteristic of H_3PO_4, whereas the peaks at −10.8 and −22.8 ppm were attributed to terminal and internal phosphate groups of condensed phosphates, respectively.[30] Krawietz et al. assigned the peak at −35.9 ppm to silicon hydrogen tripolyphosphate (−35 ppm).[31] For $H_3[PMo_{12}O_{40}]$ supported on ZrO_2 (PMo_{12}-ZrO_2), Devassy et al. investigated the nature of P species depending on Keggin loading and calcination temperature.[32] PMo_{12}-ZrO_2 exhibited a comparable broadening of the peaks in the ^{31}P MAS NMR spectrum with the increase in calcination temperature. The decomposition of HPOMs to oxide species was observed at temperatures above 723 K. López-Salinas et al investigated the thermal stability of $H_3[PW_{12}O_{40}]$ supported on ZrO_2 (PW_{12}-ZrO_2). The structural behavior of PW_{12}-ZrO_2 during calcination was comparable to that of PMo_{12}-ZrO_2. PW_{12}-ZrO_2 decomposed at temperatures above 773 K to form the corresponding supported oxides.[33] The authors assigned an additional peak at −30 ppm to phosphorous oxides exhibiting P–O–P motifs. In the ^{31}P MAS NMR spectra of activated PV_2Mo_{10}-SBA-15 studied herein, a broad resonance indicated structural rearrangement and a partial decomposition of Keggin ions during thermal treatment under catalytic conditions. Moreover, the ^{31}P MAS NMR spectra of activated PV_2Mo_{10}-SBA-15 resembled those of a VPO-SBA-15 sample treated under oxidative and reductive conditions.[34] A broad resonance observed for the VPO-SBA-15 sample between −12 and −38 ppm was attributed to various vanadyl orthophosphates phases (−8.4 to 21.2 ppm) and P bound to the SBA-15 support (≈−38 ppm). Comparable structural motifs may be assumed for activated PV_2Mo_{10}-SBA-15. However, the formation of phosphorous oxide or silicon hydrogen tripolyphosphate exhibiting linked P–O–P structures could be excluded. In total, the ^{31}P MAS NMR results indicated various structural motifs in the activated samples studied herein. Apparently, P remained connected to the molybdate and/or vanadate species of the $[(Mo,V)O_x]$ units under propene oxidation conditions.

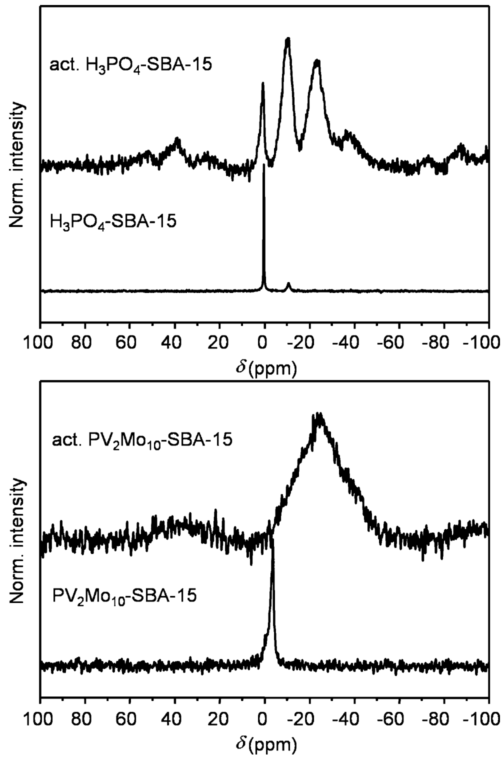

Figure 10. ^{31}P MAS NMR spectra of as-prepared H_3PO_4-SBA-15, PV_2Mo_{10}-SBA-15, activated H_3PO_4-SBA-15, and activated PV_2Mo_{10}-SBA-15 after thermal treatment in 5% propene and 5% oxygen in He at 723 K.

Structure-directing effects of V and the support material on activated PV_2Mo_{10}-SBA-15 under catalytic conditions

Characteristic differences were found on comparing the structural evolution of bulk HPOMs during thermal treatment with that of supported HPOMs. In bulk HPOMs, the Keggin ions partially decompose under catalytic conditions to form lacunary Keggin anions.[11] In this process, Mo cations migrate to extra Keggin ion sites while remaining coordinated to the resulting lacunary Keggin anions.[11] Driving force for the formation of lacunary Keggin anions may be the relaxation of the Keggin structure at an elevated temperature upon removal of structural water. Eventually, this leads to the formation of more extended oxide structures. These structural changes at temperatures above 573 K are accompanied by reduction of the metal centers.[6,11] V incorporated in bulk HPOM acts as a structural promoter facilitating the formation of the active bulk (Mo,V) oxide phase under catalytic conditions. The incorporated V centers result in a pronounced destabilization and accelerated decomposition of the Keggin ion at elevated temperatures.[5,35] The structural characteristics of model systems such as MoO_x-SBA-15 and VO_x-SBA-15 depend on their hydration states.[22,36] A comparable effect could be responsible for the structural evolution of HPOMs supported on SBA-15. Adsorbed water and silanol groups from the support may have a structure stabilizing effect on the Keggin ion. This effect would be comparable to that of water of crystallization and constitutional water in bulk HPOM under ambient conditions.[35] Vansant et al. reported that amorphous silica showed the dehydroxylation of silanol groups between 473 and 673 K, which resulted in a decrease in the silanol density from 4.6 OH nm^2 (473 K) to 2.3 OH nm^2 (673 K).[37] The thermogravimetric measurement of PV_2Mo_{10}-SBA-15 showed a mass loss of approximately 2 wt% between 473 and 673 K, which correlated with the temperature range of structural rearrangement of PV_2Mo_{10}-SBA-15 under catalytic conditions. Thus, desorption of water and dehydroxylation of silanol groups may be responsible for the formation of activated PV_2Mo_{10}-SBA-15. SBA-15 seemed to have a directing effect on the formation of activated $(Mo,V,P)O_x$ structures, depending on the treatment conditions (i.e., temperature and gas composition). Apparently, the thermal stability of Keggin ions supported on SBA-15 was significantly decreased. Although V had a minor effect on the thermal stability, the interaction with the support material appeared to be more important. Nevertheless, V still had a distinct structure-directing effect to form V—O—Mo mixed structures under catalytic conditions. The presence of tetrahedral $[VO_4]$ species led to an increasing ratio of tetrahedral $[MoO_4]$ to octahedral $[MoO_6]$ species. Compared with SBA-15, other support materials exhibit different structure-directing effects, depending on the acidity of the surface.[16,38,39] For instance, mainly isolated $[MoO_4]$ units existed on an alkaline MgO support, which was in agreement with the behavior of molybdenum oxides in the alkaline solution.[24] Herein, the acidic surface of silica SBA-15 resulted in mainly linked M—O—M (M = Mo, V) species, which was again in agreement with the behavior of vanadates and molybdates in acidic solutions.[40,41]

Catalytic performance

Reaction rates and selectivities of PV_2Mo_{10}, PV_2Mo_{10}-SBA-15, and $V_2Mo_{10}O_x$-SBA-15 in propene oxidation at 723 K are illustrated in Figure 11. Bulk PV_2Mo_{10} and PV_2Mo_{10}-SBA-15 exhibited a comparable product distribution (i.e., acrylic acid, acetic acid, acrolein, acetone, propionaldehyde, acetaldehyde, CO, and CO_2). Although PV_2Mo_{10} showed a slightly increased selectivity toward acrolein, PV_2Mo_{10}-SBA-15 exhibited an increased selectivity toward acetic acid. The total oxidation products CO and CO_2 amounted to approximately 55% in the resulting oxidation products. Conversely, the reaction rates of PV_2Mo_{10} and PV_2Mo_{10}-SBA-15 exhibited considerable differences. The catalytic activity of PV_2Mo_{10}-SBA-15 was four times higher than that of bulk PV_2Mo_{10}. Apparently, higher dispersion and an improved surface to bulk ratio of Keggin ions resulted in a much increased activity at comparable selectivity. In contrast to the HPOMs samples, $V_2Mo_{10}O_x$-SBA-15 showed a decreasing activity and a different product distribution as compared with PV_2Mo_{10}-SBA-15. Although the amount of total oxidation products in the gas phase was considerably lower, an increasing selectivity toward acetaldehyde was determined. The structural analysis indicated that activated $V_2Mo_{10}O_x$-SBA-15 had an increased amount of highly polymerized Mo species and a decreased amount of tetrahedral $[MoO_4]$ units. It was shown earlier that highly polymerized $[VO_x]$ and $[MoO_x]$ species showed an increased selectivity toward oxidation products.[24,42] In addition, the majority of $[VO_x]$ and $[MoO_x]$ species in activated $V_2Mo_{10}O_x$-SBA-15 did not seem to be directly connected to each other. Local separation of $[VO_x]$ and $[MoO_x]$ species may be responsible for the increased concentration of acetaldehyde, which is mainly formed by V-based catalysts in contrast to Mo-based catalysts.[1,21,42] Apparently, connected $[VO_4]$ and $[MoO_x]$ units led to an increased amount of total oxidation products for activated PV_2Mo_{10}-SBA-15 in contrast to not connected $[VO_4]$ and $[MoO_x]$ units in activated $V_2Mo_{10}O_x$-SBA-15. Furthermore, the availability of dimeric or oligomeric $[(V,Mo)O_x]$ units increased the selectivity toward oxygenates in contrast to isolated $[MoO_4]$ units.[24,42]

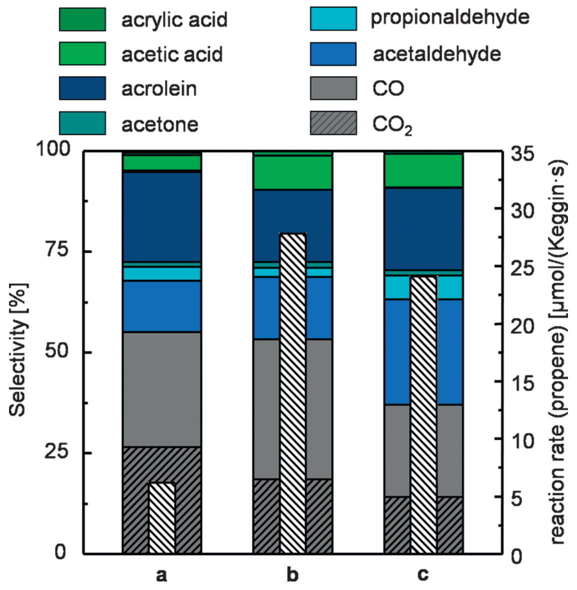

Figure 11. Reaction rate (propene) and selectivity of a) PV_2Mo_{10}, b) PV_2Mo_{10}-SBA-15, and c) $V_2Mo_{10}O_x$-SBA-15 in 5% propene and 5% oxygen in He at 723 K.

Effect of P species on catalytic activity

P-containing catalysts (i.e., VPO, FePO, and MoPO) play a crucial role as oxidation catalysts.[7] Adding small amounts of phosphoric acid to the feed showed positive effects on long-term stability and catalytic performance of FePO catalysts during the ODH of isobutyric acid to methacrylic acid. The P source was needed to maintain a constant P/Fe ratio at the surface of the catalyst.[43] VPO catalysts showed the migration of P species to the surface and a decreasing amount of P in the catalyst during water vapor treatment. The excess of P on the surface suppressed the oxidation of VPO catalysts and hindered the formation of active sites for oxidation reactions. Subsequently, the hydrolysis of P–O–P or P–O–V groups resulted in a removal of phosphate groups from the surface and an increasing activity.[7,44] Moreover, adding V and P to MoO_x-based catalysts for the ODH of ethane afforded an increasing conversion and selectivity toward ethane. Haddad et al. suggested synergistic effects between structurally related oxides such as $(V,Mo)_5O_{14}$ and (V,Mo)PO phases to be responsible for the enhanced catalytic performance.[8] Herein, the formation of water as a by-product during the oxidation of propene may have favored the migration of P species under catalytic conditions. The different surface to bulk ratios of PV_2Mo_{10} and PV_2Mo_{10}-SBA-15 could lead to a different migration pattern and hydrolysis of phosphate groups in the materials. The available Keggin ions in PV_2Mo_{10}-SBA-15 were already located on the surface of the support material. Therefore, a possible enrichment of phosphate groups was not possible for PV_2Mo_{10}-SBA-15. An enrichment of phosphate groups on the surface of bulk PV_2Mo_{10} would result in a higher P/M (M = Mo, V) ratio, with a possible effect on catalytic activity and selectivity. However, the comparable selectivity of bulk PV_2Mo_{10} and PV_2Mo_{10}-SBA-15 (Figure 11) was indicative of similar active centers despite different P/M (M = Mo, V) ratios. Therefore, the increased catalytic activity of PV_2Mo_{10}-SBA-15 was attributed to higher dispersion and an improved surface to bulk ratio of supported Keggin ions.

Conclusions

The structural evolution of PV_2Mo_{10}-SBA-15 and reference $V_2Mo_{10}O_x$-SBA-15 under propene oxidation conditions was examined by using in situ X-ray absorption spectroscopy at the Mo and V K edge. In addition, ^{31}P MAS NMR measurements of supported PV_2Mo_{10}-SBA-15 and H_3PO_4-SBA-15 were performed after the catalytic reaction. During thermal treatment under propene oxidation conditions, PV_2Mo_{10}-SBA-15 formed a mixture of mainly tetrahedral $[MoO_x]$ and $[VO_x]$ units. Changes in the average local structure around V centers coincided with the changes in the average local structure around Mo centers and the onset of catalytic activity. Apparently, mainly tetrahedral $[MoO_x]$ and $[VO_x]$ units were in close proximity and interacted under catalytic conditions. Conversely, structural analysis of the activated reference $V_2Mo_{10}O_x$-SBA-15 synthesized with individual V and Mo precursors indicated that $[VO_x]$ and $[MoO_x]$ species were mostly separated from each other on the surface of SBA-15. Moreover, activated $V_2Mo_{10}O_x$-SBA-15 had an increased amount of highly polymerized $[MoO_x]$ species and a decreased amount of tetrahedral $[MoO_4]$ units, which may explain the observed increased selectivity toward partial oxidation products. The structural environment of P in PV_2Mo_{10}-SBA-15 under catalytic conditions corresponded to a mixture of various species. P was linked to both the SBA-15 support via P–O–Si bonds and the Mo or V centers of $[MoO_x]$ or $[VO_x]$ units. In total, supported V-substituted Keggin ions are suitable precursors to synthesize $[VO_x]$ species connected to $[MoO_x]$ species on SBA-15. Apparently, the proximity of V and Mo in Keggin precursors is a prerequisite for obtaining connected metal oxide species.

Experimental Section

Silica SBA-15 was prepared according to the method of Zhao et al.[15] A triblock copolymer (16.2 g; P123, Aldrich) was dissolved in water (294 g) and hydrochloric acid (8.8 g) at 308 K and stirred for 24 h. After the addition of tetraethyl orthosilicate (32 g) for 24 h, the reaction mixture was stirred for 24 h at 373 K. The resulting gel was transferred to a glass bottle, and the closed bottle was heated to 388 K for 24 h. Subsequently, the suspension was filtered and washed with a mixture of water and ethanol (100:5). The resulting white powder was dried at 378 K for 3 h and calcined at 453 K for 3 h and at 823 K for 5 h.

HPOM were prepared as follows[5]: MoO_3 (16.89 g; Sigma–Aldrich) and V_2O_5 (2.13 g; Sigma–Aldrich) were dissolved in water (675 mL) and heated to reflux. Phosphoric acid (97.8 mL, 0.12 M) was added dropwise to the reaction mixture. The resulting suspension was heated for 3 h and kept at 298 K for 24 h until a clear red solution was obtained. The remainder was filtered, and the volume of the resulting red solution was reduced to 30 mL with an evaporator. $H_5[PV_2Mo_{10}O_{40}]$ (denoted as PV_2Mo_{10}) crystallized during storage at 277 K for several days. PV_2Mo_{10} supported on silica SBA-15 (denoted as PV_2Mo_{10}-SBA-15) was prepared through incipient wetness impregnation. PV_2Mo_{10} (0.781 g) was dissolved in water (6 mL) and deposited on silica SBA-15 (3 g) to obtain a loading of 10 wt% Mo and 1 wt% V.
A reference material (denoted as $V_2Mo_{10}O_x$-SBA-15) was prepared as follows: $(NH_4)_6Mo_7O_{24}\cdot 4H_2O$ (232.1 mg) and $(NH_4)_6V_{10}O_{28}\cdot 6H_2O$ (29.3 mg) were dissolved in water and were deposited through incipient wetness impregnation on SBA-15 (1 g) to obtain a metal loading of 10 wt% Mo and 1 wt% V. The sample was dried at RT for 18 h and calcined at 773 K for 3 h. H_3PO_4-SBA-15 was prepared by depositing phosphoric acid (1.1 mL, 0.12 M) on silica SBA-15 (1 g).

N_2 physisorption isotherms were measured at 77 K on a BELSORP-Mini II volumetric sorption analyzer (BEL Japan, Inc.). The silica SBA-15 sample was treated under vacuum at 368 K for approximately 20 min and at 448 K for approximately 17 h before starting the measurement. Data processing was performed with the BELMaster V.5.2.3.0 software package. The specific surface area was calculated by using the BET method in the relative pressure range of 0.03–0.24 by assuming an area of 0.162 nm^2 per N_2 molecule.[45] The adsorption branch of the isotherm was used to calculate the pore size distribution and cumulative pore area according to the BJH method.[46]

The ^{31}P MAS NMR spectra were recorded on a Bruker Avance 400 MHz NMR spectrometer (161.92 MHz) with a 4 mm double resonance HX MAS probe. Data collection used a 90° pulse with a relaxation delay of 60 s under an MAS rotation frequency of 12 kHz. The spectra were referenced to 85% H_3PO_4 in aqueous solution with solid $NH_4H_2PO_4$ ($\delta = 0.81$ ppm) as a secondary reference.

XRD measurements were performed on an X'Pert PRO multipurpose diffractometer (PANalytical, θ–θ geometry) with CuK$_\alpha$ radiation and a PIXcel solid-state multichannel detector. Wide-angle scans ($2\theta = 5$–90°, variable slits) were collected in the reflection mode with a silicon sample holder. Small-angle scans ($2\theta = 0.4$–6.0°, fixed slits) were collected in the transmission mode with the sample spread between two layers of Kapton foil.

Transmission XAS experiments at the Mo K edge (19.999 keV) were performed at beamline X at the Hamburg Synchrotron Radiation Laboratory with a Si(311) double crystal monochromator. Transmission XAS experiments at the V K edge (5.465 keV) were also performed at the Hamburg Synchrotron Radiation Laboratory with a Si(111) double crystal monochromator at beamline C. In situ experiments were performed in a flow reactor at atmospheric pressure (5 vol% oxygen in He; total flow rate: 30 mL min^{-1}; temperature range: 303–723 K; heating rate: 4 K min^{-1}). The gas phase composition at the cell outlet was monitored continuously with a noncalibrated mass spectrometer in a multiple ion detection mode (OmniStar from Pfeiffer).

XAFS analysis was performed with the WinXAS v3.2 software package.[47] Background subtraction and normalization were performed by fitting linear polynomials and third-degree polynomials to the pre-edge and post-edge region of an absorption spectrum, respectively. The EXAFS $\chi(k)$ was extracted by using cubic splines to obtain a smooth atomic background $\mu_0(k)$. The FT($\chi(k)\cdot k^3$), often referred to as pseudo radial distribution function, was calculated by Fourier transforming the k^3-weighted experimental $\chi(k)$ function, multiplied by a Bessel window, in the R space. EXAFS data analysis was performed by using theoretical backscattering phases and amplitudes calculated with the ab initio multiple scattering code FEFF7.[48]

Single scattering and multiple scattering paths in the hexagonal MoO_3 model structure (ICSD no. 75417[49]) and a modified Na_2MoO_4 structure (ICSD no. 24312[25]) were calculated up to 6.0 Å with a lower limit of 4.0% in amplitude with respect to the strongest backscattering path. EXAFS refinements were performed in the R space simultaneously to magnitude and imaginary part of a Fourier transformed k^3-weighted and k^1-weighted experimental $\chi(k)$ function by using the standard EXAFS formula.[50] This procedure reduced the correlation between the various XAFS fitting parameters. Structural parameters allowed to vary in the refinement were 1) disorder parameter σ^2 of selected single scattering paths assuming a symmetrical pair distribution function and 2) distances of selected single scattering paths. Correlations of specific parameters to reduce the number of free running parameters and to improve the stability of the refinement are given in Tables 1 and 2.

The statistical significance of the fitting procedure used was carefully evaluated in three steps as outlined by Walter et al.[22] The procedure took into account the recommendations of the International X-ray Absorption Society on criteria and error reports.[51] First, the number of independent parameters (N_{ind}) was calculated by using the Nyquist theorem: $N_{ind} = 2/\Pi^*\Delta R^*\Delta k + 2$. In all cases, the number of free running parameters in the refinements was well below N_{ind}. Second, confidence limits were calculated for each individual parameter. In the corresponding procedure, one parameter was successively varied by a certain percentage (i.e., 0.05% for R and 5% for σ^2) and the refinement was restarted by keeping this parameter constant. The parameter was repeatedly increased or decreased until the fit residual exceed the original fit residual by more than 5%. Eventually, the confidence limit of the parameter was obtained from linear interpolation between the last and the second last increment for an increase in fit residual of 5%. This procedure was consecutively performed for each fitting parameter. Third, an F test was performed to assess the significance of the effect of additional parameters on the fit residual.[52]

Quantitative catalysis measurements were performed with a fixed-bed laboratory reactor connected to an online GC system (Varian CP-3800) and a noncalibrated mass spectrometer (OmniStar from Pfeiffer). All gas lines and valves were preheated to 473 K. Hydrocarbons and oxygenated reaction products were analyzed with a Carbowax capillary column connected to an Al_2O_3/MAPD column or a fused silica restriction capillary (25 m×0.32 mm each) connected to a flame ionization detector. O_2, CO, and CO_2 were separated with HayeSep Q (2 m×1/8 in.) and HayeSep T (0.5 m×1/8 in.) packed columns as precolumns combined with a back flush. For separation, a Hayesep Q packed column (0.5 m×1/8 in.) was connected via a molecular sieve (1.5 m×1/8 in.) to a thermal conductivity detector. Reactant gas flow rates of oxygen, propene, and He were adjusted with separate mass flow controllers to a total flow of 40 mL min^{-1}. A mixture of 5% propene and 5% oxygen in He was used for catalytic testing in the temperature range 300–723 K.

Acknowledgements

We acknowledge the Hamburg Synchrotron Radiation Laboratory for providing beamtime for this work. We are grateful to Dr. J. Scholz, A. Müller, S. Kühn, and G. Koch for contributing to the characterization of the materials. We also acknowledge financial support from the Deutsche Forschungsgemeinschaft (DFG).

Keywords: EXAFS spectroscopy · heterogeneous catalysis · molybdenum · structure–activity relationships · vanadium

[1] B. Grzybowska-Świerkosz, *Top. Catal.* **2000**, *11/12*, 23–42.
[2] M. Bettahar, G. Costentin, L. Savary, J. Lavalley, *Appl. Catal. A* **1996**, *145*, 1–48.
[3] R. Schlögl, *Top. Catal.* **2011**, *54*, 627–638.
[4] T. Ressler, O. Timpe, F. Girgsdies, *Z. Kristallogr.* **2005**, *220*, 295–305.
[5] T. Ressler, O. Timpe, F. Girgsdies, J. Wienold, T. Neisius, *J. Catal.* **2005**, *231*, 279–291.
[6] T. Ressler, O. Timpe, *J. Catal.* **2007**, *247*, 231–237.
[7] A. Maiti, N. Govind, P. Kung, D. King-Smith, J. E. Miller, C. Zhang, G. Whitwell, *J. Chem. Phys.* **2002**, *117*, 8080–8088.
[8] N. Haddad, E. Bordes-Richard, A. Barama, *Catal. Today* **2009**, *142*, 215–219.
[9] N. Mizuno, M. Misono, *Chem. Rev.* **1998**, *98*, 199–218.
[10] H.-G. Jerschkewitz, E. Alsdorf, H. Fichtner, W. Hanke, K. Jancke, G. Öhlmann, *Z. Anorg. Allg. Chem.* **1985**, *526*, 73–85.
[11] J. Wienold, O. Timpe, T. Ressler, *Chem. Eur. J.* **2003**, *9*, 6007–6017.
[12] I. E. Wachs, *Catal. Today* **2005**, *100*, 79–94.
[13] C. Hess, *J. Catal.* **2007**, *248*, 120–123.
[14] D. Zhao, J. Feng, Q. Huo, N. Melosh, G. H. Friedrickson, B. F. Chmelka, G. D. Stucky, *Science* **1998**, *279*, 548–552.
[15] D. Zhao, Q. Huo, J. Feng, B. F. Chmelka, G. D. Stucky, *J. Am. Chem. Soc.* **1998**, *120*, 6024–6036.
[16] D. E. Keller, D. C. Koningsberger, B. M. Weckhuysen, *J. Phys. Chem. B* **2006**, *110*, 14313–14325.
[17] G. M. Dhar, G. M. Kumaran, M. Kumar, K. S. Rawat, L. D. Sharma, B. D. Raju, K. R. Rao, *Catal. Today* **2005**, *99*, 309–314.
[18] T. Ressler, U. Dorn, A. Walter, S. Schwarz, A. Hahn, *J. Catal.* **2010**, *275*, 1–10.
[19] J. Boeyens, G. McDougal, J. Van R. Smit, *J. Solid State Chem.* **1976**, *18*, 191–199.
[20] T. Ressler, J. Wienold, R. Jentoft, T. Neisius, *J. Catal.* **2002**, *210*, 67–83.

[21] S. Kühn, P. Schmidt-Zhang, A. H. P. Hahn, M. Huber, M. Lerch, T. Ressler, *Chem. Cent. J.* **2011**, *5*, 42 – 52.
[22] A. Walter, R. Herbert, C. Hess, T. Ressler, *Chem. Cent. J.* **2010**, *4*, 3 – 23.
[23] J. P. Thielemann, T. Ressler, A. Walter, G. Tzolova-Müller, C. Hess, *Appl. Catal. A* **2011**, *399*, 28 – 34.
[24] J. Scholz, A. Walter, A. Hahn, T. Ressler, *Microporous Mesoporous Mater.* **2013**, *180*, 130 – 140.
[25] M. Seleborg, R. G. Hazell, Å. Nilsson, J. Sandström, H. Theorell, R. Blinc, S. Paušak, L. Ehrenberg, J. Dumanović, *Acta Chem. Scand.* **1967**, *21*, 499 – 504.
[26] R. K. Grasselli, *Top. Catal.* **2002**, *21*, 79 – 88.
[27] K. Inumaru, A. Ono, H. Kubo, M. Misono, *Faraday Trans.* **1998**, *94*, 1765 – 1770.
[28] R.-Y. Wang, D.-Z. Jia, L. Zhang, L. Liu, Z.-P. Guo, B.-Q. Li, J.-X. Wang, *Adv. Funct. Mater.* **2006**, *16*, 687 – 692.
[29] Z. Zhang, Y. Qu, S. Wang, J. Wang, *Chin. J. Chem. Phys.* **2009**, *22*, 315 – 321.
[30] M. M. Crutchfield, C. V. Callis, R. R. Irani, G. C. Roth, *Inorg. Chem.* **1962**, *1*, 813 – 817.
[31] T. R. Krawietz, P. Lin, K. E. Lotterhos, P. D. Torres, D. H. Barich, A. Clearfield, J. F. Haw, *J. Am. Chem. Soc.* **1998**, *120*, 8502 – 8511.
[32] B. M. Devassy, F. Lefebvre, W. Böhringer, J. Fletcher, S. B. Halligudi, *J. Mol. Catal. A* **2005**, *236*, 162 – 167.
[33] E. López-Salinas, J. Hernández-Cortéz, I. Schifter, E. Torres-García, J. Navarrete, A. Gutiérrez-Carrillo, T. López, P. Lottici, D. Bersani, *Appl. Catal. A* **2000**, *193*, 215 – 225.
[34] J. Frey, C. Lieder, T. Schölkopf, T. Schleid, U. Nieken, E. Klemm, M. Hunger, *J. Catal.* **2010**, *272*, 131 – 139.
[35] L. Marosi, E. Escalona Platero, J. Cifre, C. Otero Areán, *J. Mater. Chem.* **2000**, *10*, 1949 – 1955.
[36] T. Ressler, A. Walter, Z. Huang, W. Bensch, *J. Catal.* **2008**, *254*, 170 – 179.
[37] E. F. Vansant, P. van der Voort, K. C. Vrancken, *Characterization and chemical modification of the silica surface, Vol. 93*, Elsevier, Amsterdam, New York, **1995**.
[38] R. Radhakrishnan, C. Reed, S. T. Oyama, M. Seman, J. N. Kondo, K. Domen, Y. Ohminami, K. Asakura, *J. Phys. Chem. B* **2001**, *105*, 8519 – 8530.
[39] J. Handzlik, P. Sautet, *J. Phys. Chem. C* **2010**, *114*, 19406 – 19414.
[40] G. Deo, I. E. Wachs, J. Haber, *Crit. Rev. Surf. Chem.* **1994**, *4*, 141 – 187.
[41] K. F. Jahr, J. Fuchs, *Angew. Chem.* **1966**, *78*, 725 – 735.
[42] J. Scholz, A. Walter, T. Ressler, *J. Catal.* **2014**, *309*, 105 – 114.
[43] J.-M. M. Millet, *Catal. Rev. Sci. Eng.* **1998**, *40*, 1 – 38.
[44] F. Richter, H. Papp, T. Götze, G. Wolf, B. Kubias, *Surf. Interface Anal.* **1998**, *26*, 736 – 741.
[45] S. Brunauer, P. H. Emmett, E. Teller, *J. Am. Chem. Soc.* **1938**, *60*, 309 – 319.
[46] E. P. Barrett, L. G. Joyner, P. P. Halenda, *J. Am. Chem. Soc.* **1951**, *73*, 373 – 380.
[47] T. Ressler, *J. Synchrotron Radiat.* **1998**, *5*, 118 – 122.
[48] J. J. Rehr, C. H. Booth, F. Bridges, S. I. Zabinsky, *Phys. Rev. B* **1994**, *49*, 12347 – 12350.
[49] J.-D. Guo, P.Yu. Zavalij, M. S. Whittingham, *J. Solid State Chem.* **1995**, *117*, 323 – 332.
[50] T. Ressler, S. L. Brock, J. Wong, S. L. Suib, *J. Phys. Chem. B* **1999**, *103*, 6407 – 6420.
[51] *StandardsCriteria_July25_2000*, to be found under http://www.ixasportal.net/ixas/images/ixas_mat/StandardsCriteria_July25_2000.pdf.
[52] W. H. Press, *Numerical recipes. The art of scientific computing, 3rd ed.*, Cambridge University Press, Cambridge, **2007**.

Received: December 4, 2014
Revised: January 17, 2015